Chinese Journal of Electronics
vol. 33, no. 2, pp. 516–526, March 2024
https://doi.org/10.23919/cje.2023.00.039

RESEARCH ARTICLE

A Compact Filtering Antenna System with Wide-Angle Scanning Capability for V2I Communication

Chuang HAN[1], Tong LI[1], Zhaolin ZHANG[1], Ling WANG[1], and Guangwei YANG[2]

1. *School of Electronics and Information, Northwestern Polytechnical University, Xi'an 710072, China*
2. *School of Electronic Engineering and Computer Science, Queen Mary University of London, London, E1 4NS, UK*

Corresponding author: Guangwei YANG, Email: gwyang086@gmail.com
Manuscript Received February 11, 2023; Accepted May 23, 2023

Abstract — A compact filtering antenna system with wide-angle scanning is proposed for vehicle to infrastructure (V2I) communication which would handle complex communication scenarios. In this work, a wide beam filtering antenna is realized by using some inductive resistance structures such as metal pins and pillars, and capacitive structures such as slots, parasitical patches to produce the radiation nulls at two sides of the operating frequency band and improve the impedance matching in the passband. Meanwhile, the wide beam capability is also realized by the above structure. Furthermore, two H- and E-plane linear arrays are designed for the beam scanning capability with filtering characteristics based on the proposed antenna. To verify the proposed design concept, a prototype is fabricated and measured. The measurement and simulation agree well, demonstrating an excellent filtering characteristic with the operating frequency band from 3.18 to 3.45 GHz (about 8.1%), the high total efficiency of about 88%, and 3-dB-beamwidth of more than 100° and 120° in the above two arrays, respectively. Additionally, the proposed arrays can realize the beam scanning up to the coverage of 112° and 120° with a lower gain reduction and a good filtering characteristic, respectively.

Keywords — Filtering antenna, Wide beam, Beam scanning, Beam steering, Phased array.
Citation — Chuang HAN, Tong LI, Zhaolin ZHANG, *et al.*, "A Compact Filtering Antenna System with Wide-Angle Scanning Capability for V2I Communication," *Chinese Journal of Electronics*, vol. 33, no. 2, pp. 516–526, 2024. doi: 10.23919/cje.2023.00.039.

I. Introduction

The wireless communication systems are facing huge challenges due to the explosion of user growth in consumer wireless terminal devices including the Internet of things (IoT) [1], intelligent transportation system (ITS) [2], [3], mobile communication [4], vehicle to everything (V2X) [5], [6], imaging sensors, intelligent city (or home), etc. Therefore, this would require higher requirements in the capacity, latency, and reliability of the communication system. Recently, a variety of antennas, as the pivotal device, have been used into vehicle communication systems to meet the above requirements [7]–[12]. But in the face of high-speed mobile systems, the above antennas have serious drawbacks, which can't realize the beam scanning capability [13], [14] for mobile terminals. Hence, wide-angle beam scanning technology has become a popular research topic and is applied to modern communication systems. The wide-angle scanning antenna for vehicle to infrastructure (V2I) needs to be directional, have a wide coverage area, high sensitivity, low interference, durability, and easy installation to effectively capture data from vehicles and infrastructure devices in a variety of environments. For the wide-angle beam-scanning technology, at present, there are the following main design approaches to be adopted. From the array far-field pattern equation, it is achieved by multiplying the array factor and array unit pattern, so the first way is to broaden the antenna unit's radiating pattern, mainly such as artificial magnetic conductor (AMC) [15], designing metallic cavity structure [16], putting the metallic walls at the side of the patch [17], and so on. The second solution is using pattern-reconfigurable method to extend the array scanning range, where is achieved by microstrip

Associate Editor: Prof. Yikai CHEN, University of Eletronic Science and Technology of China.

Yagi reconfigurable antenna [18], O-slot patch antenna element controlled by the electrical components [19], combining the patch and dielectric resonator antennas [20], and so on. The third way is decoupling technology, which is achieved by the electromagnetic bandgap (EBG) structure [21], high impedance surface (HIS) [22], decoupling network [23], etc.

In addition, due to the increasing system integration, more compact and multi-functional RF front-end design is the current trend in vehicle communication system applications, especially considering the economic factors. In the past few decades, a large number of multi-functional designs aimed at integrating passive devices like filters, power dividers, and antennas have been reported [24]–[29], which could not only realize more compactness of the RF front-end subsystems but also remarkably enhance the system performance. However, there are few designs that can combine the filtering characteristic with beam scanning capability [30] for vehicle communication systems.

To address this challenge, a compact and simple wide beam filtering antenna is designed and explored in this article and applied to the phased array for wide-angle beam-scanning capability. The filtering characteristics of the proposed antenna is realized by the following method: a) The metal pins and pillars are added in the patch antenna to change the impedance performance to realize the low frequency radiation null. b) The dumbbell-shaped cross slot and parasitic patch are added in the proposed antenna to adjust its capacitive performance for realize a good high frequency radiation null. More importantly, the inverted L-shaped (IL-shaped) patch could realize two functions, which are the filtering characteristics and wide beam capability. Hence, a compact filtering antenna is design to apply for the phased array with the beam scanning capability. The proposed phased array has mutual coupling levels lower than −14.5 dB in both linear arrays, providing efficient wide-angle beam scanning with excellent filtering characteristics. This design has potential applications in vehicle communication systems.

II. The Design Processing and Mechanism Analysis

1. Configuration

The configuration of this wide beam filtering antenna is illustrated in Figure 1. It consists of the parasitic patch (Patch 2) on a thin substrate (Substrate 1) of Rogers RO4350B ($\epsilon_r = 3.66$ and $\sigma = 0.0027$, and $H_1 = 1.524$ mm), the radiating patch (Patch 1) with etching a dumbbell-shaped cross slot on a substrate (Substrate 2) ($\epsilon_r = 2.2$ and $\sigma = 0.002$, and $H_1 = 5$ mm), four inverted L-shaped patches which are set the around of the Substrate 2, and the some metallic pins. The detailed position of the metallic pins is given in Figure 1(c). The substrates are all fixed by four screws on the square floor as depicted in Figure 1(b). Also, the Patch 1 is excited by the copper probe to connect the SMA connecter. Now, the wide beam filtering antenna is designed and all dimensions of this antenna system, optimized by simulating in the Ansys software, are given in the following Table 1. The width of the dumbbell-shaped cross slot is 0.8 mm.

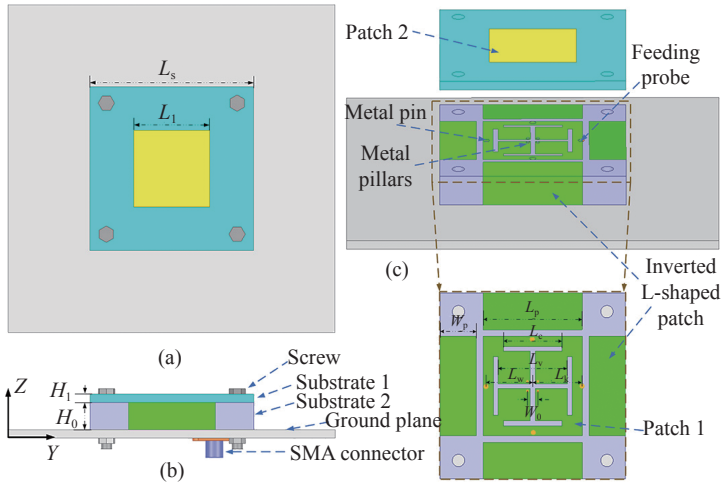

Figure 1 Geometry of this wide beam antenna with filtering characteristic. (a) Plan view; (b) Side view; (c) 3D exploded view.

Table 1 Geometrical parameters of the wide beam filtering antenna

Parameter	L_s	L_1	L_p	L_c	L_v	L_k	L_w	H_0	H_1	W_p	W_0
Value (mm)	30	14	16	8	12	7.8	7.5	5	1.524	5.9	2

2. Design evolution and mechanism

To better elaborate the antenna designing principle and understand the antenna working mechanism, the designing evolution of the wide beam filtering antenna is depicted in Figure 2, with the reference antennas being compared with the wide beam filtering antenna. All an-

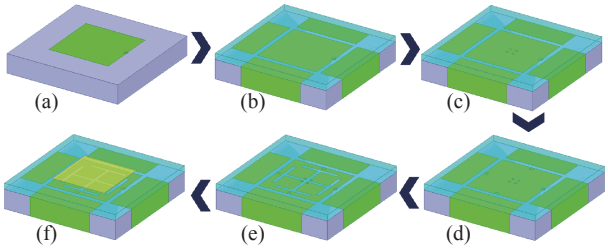

Figure 2 Evolution of the wide beam filtering antenna. (a) Antenna 0; (b) Antenna 1; (c) Antenna 2; (d) Antenna 3; (e) Antenna 4; (f) The proposed antenna.

tennas have the same parameters as given in Table 1. Their simulated *S*-parameters and realized gain with varying frequencies are reported in Figure 3 and Figure 4. From Figure 2(a), firstly, a normal microstrip antenna is designed and fed by the copper probe. Due to the small size of the patch, Antenna 0 has a higher operating frequency which is higher than 5 GHz. Hence, it is found that the input impedance of Antenna 0 is seriously mismatched in the proposed frequency band. To improve the proposed impedance characteristics and enhance the gain in this frequency band, as well as to achieve wide beam characteristics, four IL-shaped patches are employed around Substrate 2 and Substrate 1 is put on the above Patch 1 to form Antenna 1, as given in Figure 2(b). From Figure 3 and Figure 4, note that the impedance matching is realized at around 3.0 and 3.4 GHz and the radiation null at the high frequency is obtained but not well, meanwhile, the wide beam pattern is radiated in Antenna 1, as depicted in Figure 5. This is because that adding the substrate and increasing the size of radiating structure can move the resonance frequency to lower frequency band, and the vertical patch is employed to connect the ground which leads to a vertical current for broadening the beam-width and controls the capacitor between the Patch 2 and inverted L-shaped patch. However, the radiation pattern in the E-plane would be skewed to one side, due to uneven current distribution on the radiating structure. As depicted in Figure 2(c), four metallic pins are applied to improve the impedance and filtering characteristics, where form to Antenna 2. It is found that the impedance characteristic is improved a little and the filtering performance has little change as shown in Figure 3. But these pins could affect the impedance performance of the Patch 2 for the upper stopband. However, the above structures couldn't improve the lower stopband, three metal pillars are added into Antenna 2 to form Antenna 3. As given in Figure 3 and Figure 4, a narrow operating frequency band is realized and the low frequency radiation null is obtained. Because this structure could suppress the TM_{10} and produce the higher modes at the low frequency band. Therefore, this metallic pillar would influence the antenna impedance matching and filtering characteristics at low frequencies, as well as a rough wide beam filtering antenna being designed for implementation. The dumbbell-shaped cross slot is used to continue to improve the antenna performance, which are added in Antenna 3 to form Antenna 4 as depicted in Figure 2(e). The slot further optimizes the antenna impedance matching while being able to influence the filtering characteristics at the low frequency. Still, it has little effect on the filtering characteristics at the high frequency. To further improve the antenna impedance, especially the filtering characteristics at high frequencies, a parasitic patch is printed on Substrate 1 to realize the wide beam filtering antenna. As reported in Figure 3 and Figure 4, a good impedance bandwidth and two radiation nulls are ob-

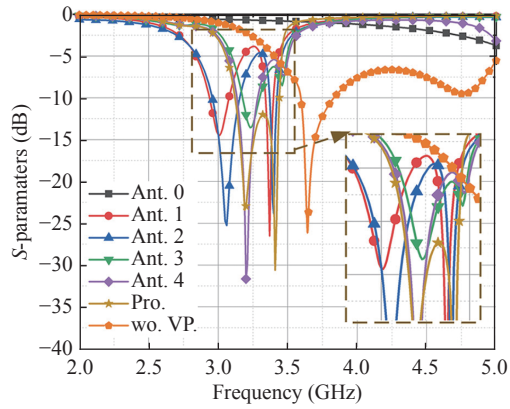

Figure 3 Simulated reflection coefficients of the reference antennas and wide beam filtering antenna (wo. VP.: without vertical part).

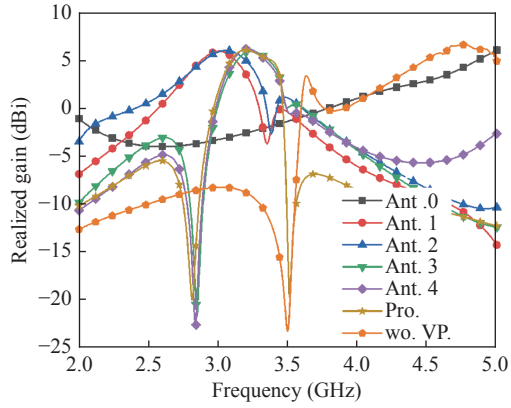

Figure 4 Simulated the realized gain of all antennas in Figure 2.

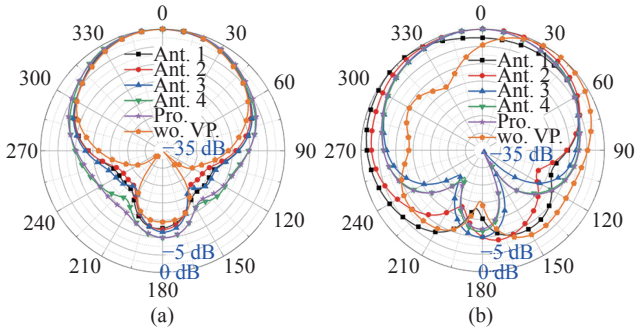

Figure 5 Simulated radiation patterns of all antennas at 3.3 GHz. (a) H-plane (*xoz*-plane); (b) E-plane (*yoz*-plane).

tained simultaneously. In addition, As the antenna structure evolves, the antenna's radiation pattern is also optimized, as given in Figure 5, especially in the E-plane, where the radiation pattern is also very symmetrical and wide beams on both sides as the current distribution becomes more symmetrical.

It is observed in Figure 4 that the antenna produces two obvious radiation nulls which are at 2.81 GHz and 3.51 GHz, respectively. To further illustrate the effect of the above key structures on the filtering and radiation performance of this antenna, this antenna's current distributions at the two radiation nulls and the resonant frequency are presented in Figure 6. From Figures 6(a) and (b), note that the horizontal current on the IL-shaped patch is oppositely oriented on the *Y*-direction and the vertical current directs to the negative *Z*-direction but the far field is cancelled because of the space distance between two vertical currents. However, these currents are induced from the radiating patch, so the distance between them would affect the current distribution on the IL-shaped patch and thus lead the low radiation null to change. Besides, like the TM_{20} mode, the horizontal currents on the radiating patch and the parasitic patch are also oppositely oriented in the *X*- and *Y*-directions. It is observed that the symmetrical metal pins and pillars and cross slot are the main causal factor of the cancelled current distribution. The high radiation null is still very important to ensure better out-of-band rejection at high frequency band. We can find that this null is at 3.51 GHz in Figure 4 and the current distribution is given in Figures 6(e) and (f). The cancelled current is also obtained on the IL-shaped patch either in the *X*- and *Y*-directions. It is different from low radiation null that the radiating patch can produce the horizontal currents which are the TM_{10} mode, while the parasitic patch is also the TM_{10} mode, but has an opposite phase. Therefore, these currents are mainly cancelled to obtain a radiation null.

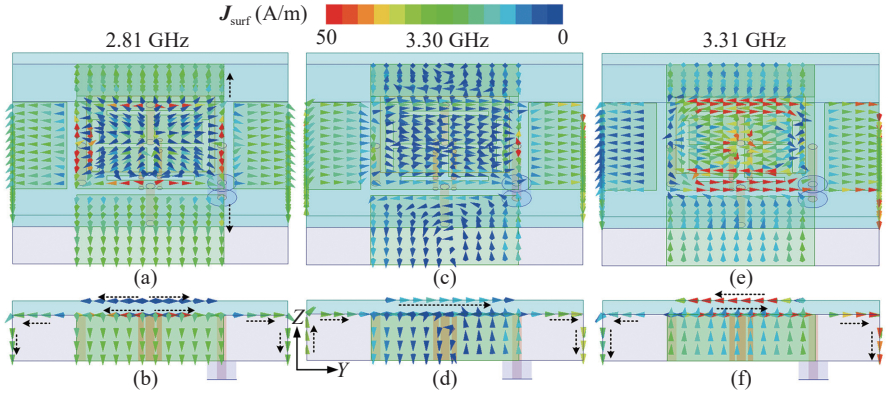

Figure 6 Current distribution of the wide beam filtering antenna. At 2.81 GHz (a) 3D view, (b) Side view; At 3.3 GHz (c) 3D view, (d) Side view; At 3.51 GHz (e) 3D view, (f) side view.

However, at the resonance frequency (3.3 GHz), the current distribution is different with the above frequencies, as given in Figures 6(c) and (d). Noted that vertical currents are obtained on the vertical patches of the IL-shaped patches, which are set on both sides of the main patch. The horizontal currents are obtained on the radiating patch and the parasitic patch. Hence, this is a typical wide beam current distribution [31], which can be gotten from

$$\boldsymbol{I} = \boldsymbol{I}_{\mathrm{h}} + \boldsymbol{I}_{\mathrm{v}} \tag{1}$$

where $\boldsymbol{I}$ is the current of the proposed antenna, which comprises of the horizontal current $\boldsymbol{I}_{\mathrm{h}}$, and the vertical current $\boldsymbol{I}_{\mathrm{v}}$. Hence, the radiating pattern of this antenna is

$$E(\theta) = A_{\mathrm{h}}F_{\mathrm{h}}(\theta) + A_{\mathrm{v}}F_{\mathrm{v}}(\theta)\left(1 + \mathrm{e}^{\mathrm{j}\delta}\right) \tag{2}$$

$F_{\mathrm{h}}(\theta)$ and $F_{\mathrm{v}}(\theta)$ represent the field-pattern functions. A_{h} and A_{v} are the amplitudes of the above two fields. δ is the phase difference of two sources. To highlight the role of the vertical part (VP) of the IL-shaped patch for extending the beam and enhancing the filtering characteristics of this antenna, we also give the *S*-parameter, gain, and radiating patterns of the designing antenna without the VP to compare with the wide beam filtering antenna, as given in Figures 3, 4, and 5, respectively. In Figure 3, it can be observed that the inductive characteristic could be obtained by connecting the vertical patch to the ground plane, which can improve the impedance matching and filtering characteristics. Meanwhile, the radiating pattern can also be improved as given in Figure 5, the antenna beam is obviously broadened, and its cross-polarization is also improved more than −20 dB in the E-plane. Therefore, considering the above analysis we can obtain a simple structural design that improves two characteristics of the antenna at the same time.

3. Parameter analysis of impedance of the antenna and radiation nulls

This wide beam filtering antenna is able to exhibit good filtering characteristics with wide beam-width by properly applied some geometric structure to adjust the antenna's inductive and capacitive characteristics. The

effect of the above structures on these characteristics of this antenna is analyzed in detail as follows.

To investigate the impedance matching and the radiation nulls of this antenna with the influence of W_0, as shown in Figure 7. Firstly, note that moving the position of the metal pins would affect the higher resonance frequency but little change the lower resonance frequency. Similarly, the low radiation null is always at 2.81 GHz and moves little with varying W_0. However, the high radiation null would move to low frequency band with increasing W_0 and the gain increases to weaken the capability of the upper stopband. Hence, this structure can service for controlling this antenna's impedance characteristic for the high radiation null. In addition, as reported in Figure 8, the slot also affects the impedance characteristic of the radiation patch, which has the same function for the antenna's impedance matching and radiation null with the metal pins. It can be found that with the slot length increasing, the proposed antenna's resonant frequency in the passband gradually moves to the low frequency band, but the impedance matching gradually becomes better and then worse. At the same time, with the increase the slot which leads to the high radiation null offsetting to the low frequency and increasing the null's gain. And it leads to weaken the upper stopband.

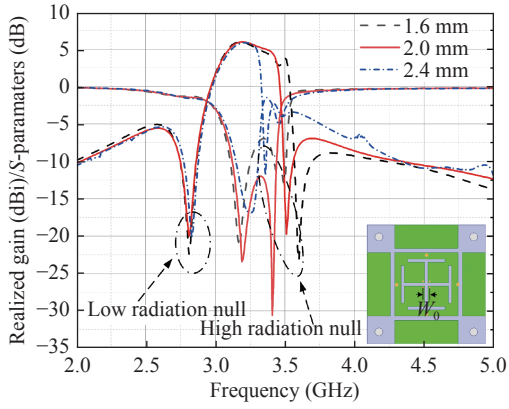

Figure 7 Simulated reflection coefficients and realized gains of the wide beam filtering antenna for different W_0.

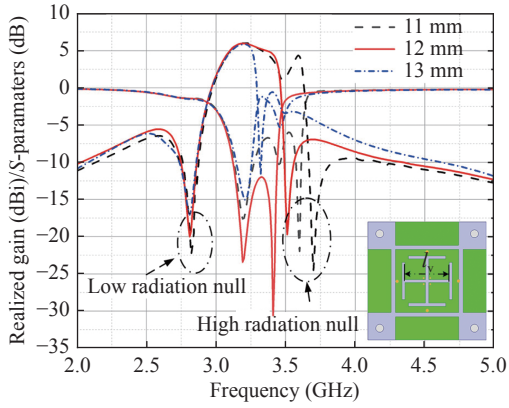

Figure 8 Simulated S-parameters and realized gains of the wide beam filtering antenna for different L_v.

Also, based on the current distribution at high radiation null, the parasitic patch plays a critical role on the upper stopband. It is demonstrated in Figure 9 that when other key parameters of the antenna remain invariant, and the parasitic patch's size (L_1) is just increased, the frequency of the high radiation null offsets to the low frequency band to result in enhancing its null gain. This is because that the resonance frequency of the parasitic patch decreases with increasing its length. In addition, like the above parameters, it has the same influence on impedance matching, both getting better first and worse later.

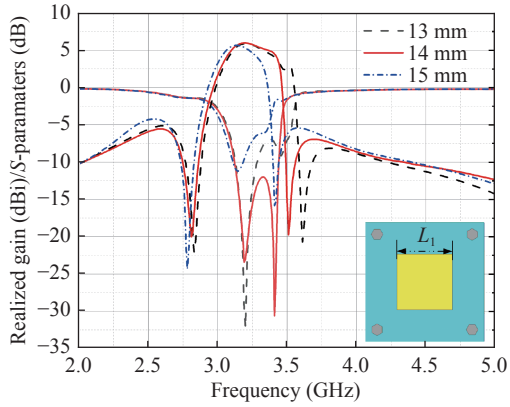

Figure 9 Simulated S-parameters and realized gains of the wide beam filtering antenna for different L_1.

For the low radiation null, as given in Figure 6(a), noted that the metal pins have a significant effect on the low radiation null, owing to their importance in the radiating patch. Hence, the position of the metal pins is investigated for realizing a sharp selectively at the lower band edge. As reported in Figure 10, with increasing L_w, the pins move to the edge of the radiating patch, the selectively becomes better first and worse later. But the null gain is enhanced. And it is little significant at the high radiation null. Besides, this antenna's impedance matching has also little effect by these parameters.

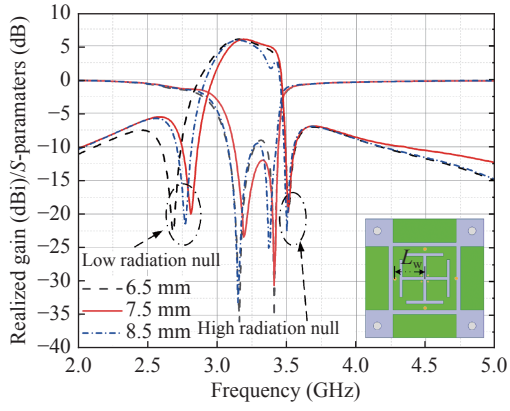

Figure 10 Simulated S-parameters and realized gains of the wide beam filtering antenna for different L_w.

From these two frequencies' current distribution of the low and high radiation nulls, it is observed that the

inverted L-shaped patch could affect the current distribution at both frequencies. As shown in Figure 11, with varying W_p, the induced current on the inverted L-shaped patch would be changed, which leads to control the cancelled currents. Hence, we would observe that with increasing W_p, the gap between the patch and the radiating patch reduces, the low radiation null offsets to lower frequency and its null gain drops. Meanwhile, the high radiation null towards to higher frequency and this null gain also drops. Because of the induced current, the in-band impedance would be also affected by this parameter. Note that it becomes better first and worse later. Besides, the wide beam characteristic will also be determined by it, as these parameters can determine the strength of the induced currents and thus the strength of the vertical currents, which in turn affects the antenna radiation characteristics.

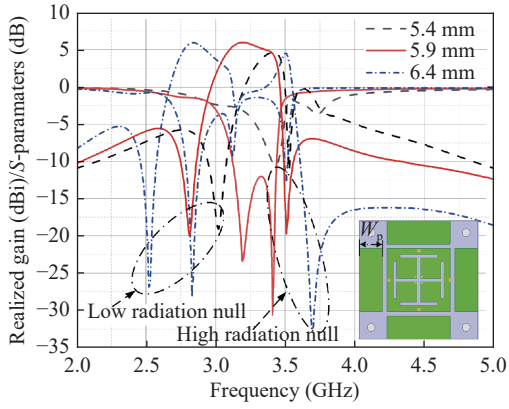

Figure 11 Simulated S-parameters and realized gains of the wide beam filtering antenna for different W_p.

4. Antenna performance

According to the above design guidance, the proposed wide beam filtering antenna is fabricated and measured. The antenna's S-parameters are implemented by a vector network analyzer. The radiating characteristics are measured in a far-field anechoic chamber. In Figure 12, the antenna's simulated and measured operating frequency bands are from 3.1 to 3.45 GHz and 3.18 to 3.45 GHz, respectively. The measured results are very similar to the simulated results, with the minor difference due to fabrication and measurement error. This figure also depicts the simulated and measured realized gain, which is very consistent across the passband. But the measured radiation nulls and the gain in the stopband have a little different from the simulations. The antenna's gain is from 5 to 6 dBi in the passband. The measured efficiency with varying frequency is also given in this figure. Noted that this antenna has a high efficiency in the passband, and little radiating power in the stopband.

The simulated and measured radiation patterns of the wide beam filtering antenna are depicted in Figure 13 and very similar. We can find that the 3 dB beamwidths in the H-plane (H-p.) reach 88° and 103° for simulation and measurement, respectively. In the E-plane (E-p.), the 3 dB beamwidths are greater than 120° for both simulation and measurement. Besides, the cross-polarization (X-pol.) in the E-plane is significantly better than the one in the H-plane and is less than 30 dB, while the cross-polarization in the H-plane is slightly worse, but also satisfies engineering applications. Hence, the good wide beam filtering antenna is realized by the proposed design principle.

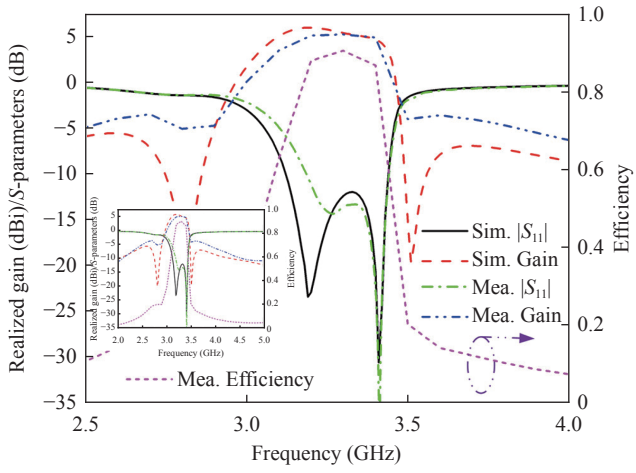

Figure 12 Simulated and measured S-parameters, realized gains, and total efficiency of the wide beam filtering antenna.

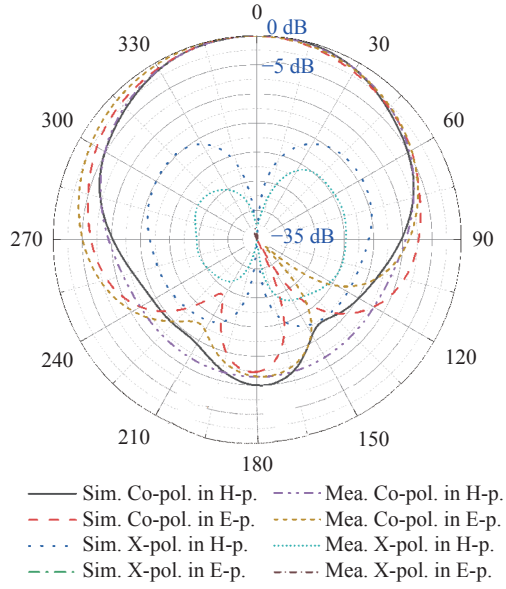

Figure 13 Simulated and measured radiation patterns of the wide beam filtering antenna at 3.3 GHz.

III. Beam Scanning Filtering Array Antenna

1. H-plane filtering array antenna

A one-to-four H-plane linear array is set to verify its beam scanning capability with the filtering characteristics in Figure 14. As all we know, for a wider scanning range, the array element-spacing should be as small as

possible, when less than half wavelength (at operating frequency), the scanning range can reach 180 degrees without the grating lobe. However, the smaller element-spacing would lead to stronger coupling between the array elements, which can be easy to affect the radiation pattern. Besides, it has higher requirements on the size of the antenna element. Fortunately, thanks to the IL-shaped patch, the structure of this antenna element becomes very compact. The array's element-spacing is set as 42 mm (lower than half wavelength at 3.5 GHz) to balance the scanning range with the coupling between the array elements. From the active element pattern [32], we assume that the coupling between each cell results in essentially the same effect and that all V_{active}. Hence, the active element pattern in the array is

$$E_{\text{active}}(\theta) = E(\theta) \cdot V_{\text{active}} \tag{3}$$

Based on the phased array principle, the array's radiation pattern is

$$E_{\text{total}}(\theta) = E_{\text{active}}(\theta) \cdot \text{AF}(\theta) \tag{4}$$

where $\text{AF}(\theta)$ is the array factor. Hence, noted that the beam scanning performance could be improved by broadening the pattern $E(\theta)$ of the array element. Meanwhile, it can also be affected by the mutual coupling in this filtering array, since the mutual coupling in this filtering array is always lower than -15 dB with good filtering characteristics, its influence for the array pattern is negligible. Besides, for the large-scale array, every E_{active} of the pattern in the array is similar, as given in equation (3). But it has some differences for small arrays, especially for edge elements. Hence, the active S-parameters of all the elements are given in the article.

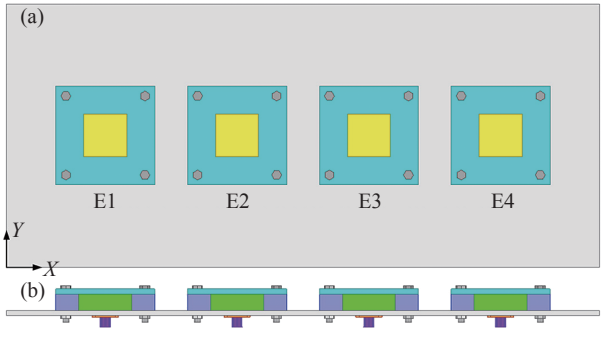

Figure 14 Configuration of H-plane linear filtering array antenna.

The active S-parameters of the array elements are presented to analyze the influence from the coupling on the scanning impedance characteristics in Figure 15. It is noted that regardless of any array elements, as the scanning angle increases, the active S-parameter gradually deteriorates, but even if the scanning reaches 56 degrees, the active S-parameter is less than -8 dB. In addition, due to the filtering characteristics, the proposed active impedance matching will not change with increasing the phase shift, resulting in the impedance frequency shifting, which is an inherent shortcoming of general phased array antennas.

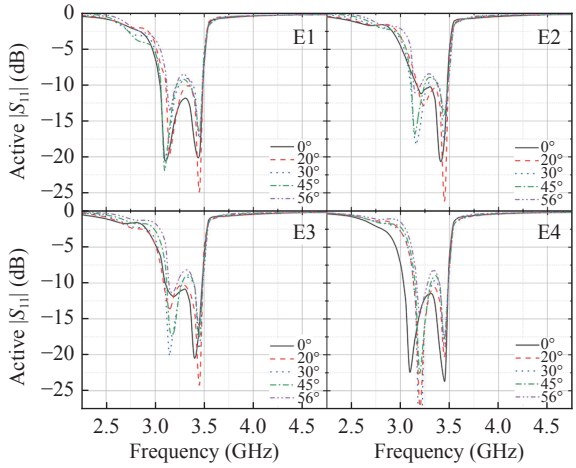

Figure 15 Simulated active S-parameters of every element in the array shown in Figure 14.

Based on this array design, the linear array prototype is fabricated as given in Figure 16. A one-to-four power driver connects the array elements and four mechanical phase shifters. The power divider and phase shifters [33] provide equal amplitude and different input phases, respectively. To verify scanning performance, the proposed H-plane linear filtering array system is assembled and tested in an anechoic chamber. The proposed feeding system, including the cable, power divider, and phase shifters, is tested separately to demonstrate the factual measured results of the proposed array. And their losses are excluded from all subsequent test results.

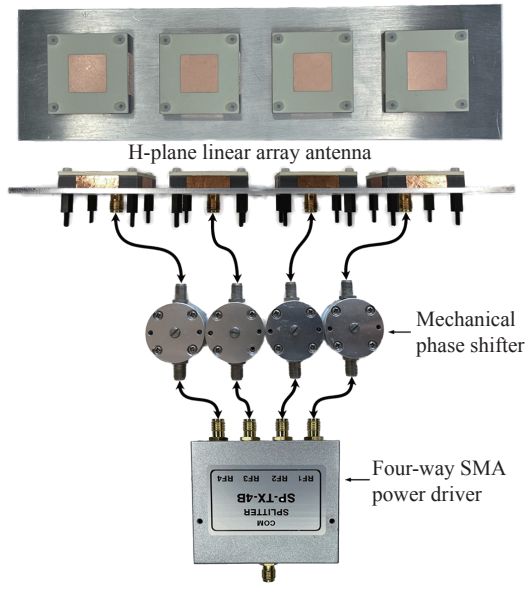

Figure 16 Prototype of the H-plane linear filtering array and measurement.

In Figure 17, this linear filtering array's measurements about its bandwidth and array coupling are presented without the feeding network and phase shifters,

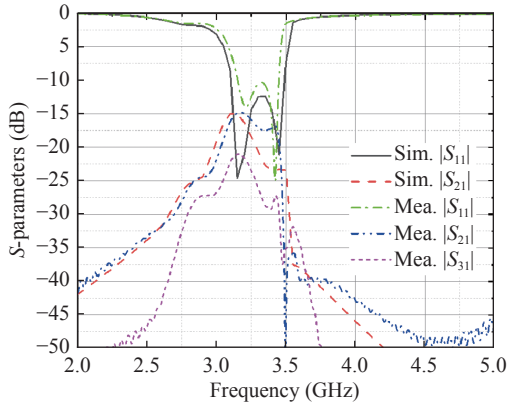

Figure 17 Simulated and measured *S*-parameters of the linear filtering array antenna.

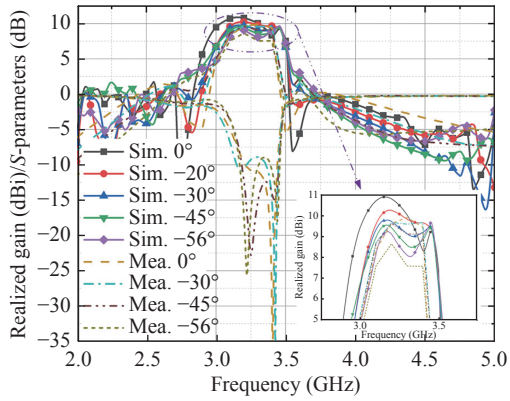

Figure 18 Simulated and measured scanning realized gain and measured scanning *S*-parameters of the H-plane linear filtering array antenna.

which agree with the simulations. The array can operate in the bandwidth from 3.18 to 3.45 GHz and has lower than −15 dB for the mutual coupling. Meanwhile, the stopband suppression looks very well from 2 to 5 GHz and the coupling in the stopband is very good, which is the main factor that causes the scanning impedance not to be frequency shifted.

According to the measurement in Figure 16, the scanning realized gain and the reflection coefficients are drawn in Figure 18. For the sake of the simplicity, four typical scanning angles are selected to verify the proposed beam scanning characteristics. Noted that the proposed filtering characteristics and wide-angle scanning capability are realized by this array antenna simultaneously. In the passband, the scanning gain drops with varying scanning angles, but the gain reduction is lower than 3 dB. Besides, the simulated and measured gains are similar and the measured gain at broadside direction is from 9.0 to 9.8 dBi. And the gain in the stopband is always lower than 0 dBi. The scanning input reflection coefficients are also shown in this figure. With varying the scanning angle from 0 degree to 56 degrees, the measured reflection coefficients are basically lower than −10 dB in the passband. For the stopband, the suppression looks very well.

Also, the scanning beams of the H-plane linear array are reported in Figure 19. It can be noted that as the scanning angle increases, the gain of the scan pattern gradually decreases. In addition, it can be found that the filtering array can achieve ±56° of scan capability and the scan gain reduction is less than 2.5 dB, and the sidelobe of the patterns is less than 7.5 dB except for the ones scanning to ±56°. The cross polarization is lower than −13 dB at any scanning angle. Four typical test scanning beams are also shown in the figure and are according with the simulations. The total efficiency of the above scanning patterns is also depicted in Figure 20. Noted that the total efficiency is very stable in the passband regardless of any scanning angles, and around −1.3 dB in the bandwidth. In the stopband, it has a low efficiency and the filtering characteristics is obviously realized by this filtering array.

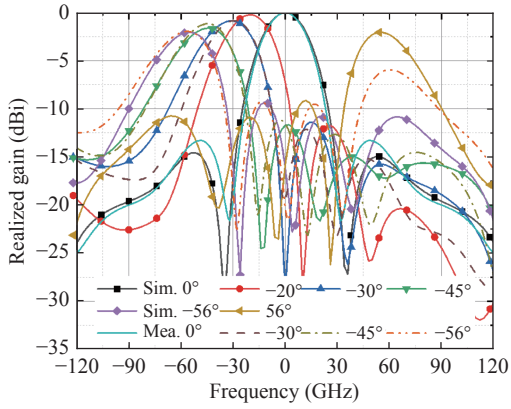

Figure 19 Simulations and measurements on the scanning beams of the H-plane linear filtering array antenna at 3.3 GHz.

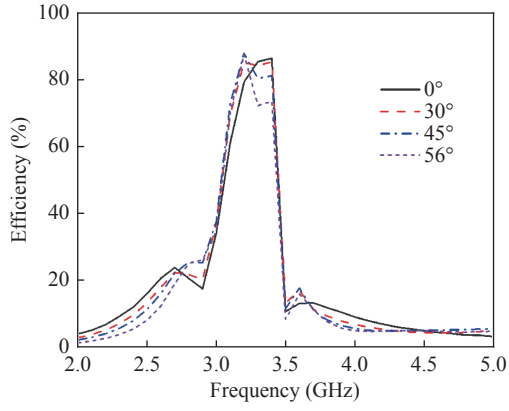

Figure 20 Measured scanning total efficiencies of the H-plane linear filtering array.

2. E-plane filtering array antenna

Similarly, a one-to-four E-plane linear filtering array is designed to verify its beam scanning capability and the filtering characteristics, which has the same element-spacing with the above linear filtering array. In Figure 21, the active *S*-parameters of the array elements in Figure 22

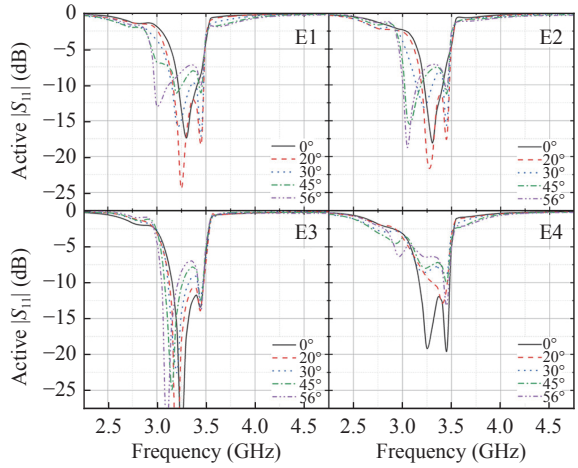

Figure 21 Simulated active *S*-parameters of every element in the array in Figure 22.

are reported to analyze the scanning impedance. Compared with the active *S*-parameters of the H-plane array antenna, the active *S*-parameters have obviously variation with enlarging the scanning angle. The active *S*-parameters vary significantly and get worse as the scan angle increases, especially for array element 4, overall, they are less than −7 dB. Comparing with the H-plane array, it reveals a slightly poorer active *S*-parameters, mainly because the coupling in the E-plane has a greater impact on the impedance matching in the array. However, the filtering characteristics of the E-plane array are also realized and don't shift with increasing scan angle, which would be given in Figure 23. This linear array is fabricated and measured by connecting a one-to-four power driver connects and four mechanical phase shifters, as depicted in Figure 22. Also, the whole antenna system is measured in the anechoic chamber to verify the scanning performance. Similarly, the operating frequency band and coupling of this linear filtering array are depicted in Figure 24. It is observed that its simulations and measurements are very similar, which is from around 3.18 to 3.45 GHz for the bandwidth, and lower than 14.5 dB for the mutual coupling in the array. More importantly, a good filtering characteristic is realized, which is low coupling in the stopband.

As demonstrated in Figure 23, the measurement results of scanning gain and input impedance at varying frequencies are presented. The findings indicate that the passband gain remains stable, exhibiting a reduction of less than 3 dB with varying beam directions. This performance aligns with the simulated results, with low and high radiation peaks observed at 2.81 GHz and 3.51 GHz, respectively. Although the measured results do not surpass the simulated ones, the stopband suppression remains robust in both cases. The scanning impedance presents a satisfactory performance, exhibiting a good passband and stopband across all scanning angles, with the passband impedance deteriorating but still remaining below −7 dB at 60° scanning angle. Figure 25 displays the scanning patterns of the filtering array at 3.3

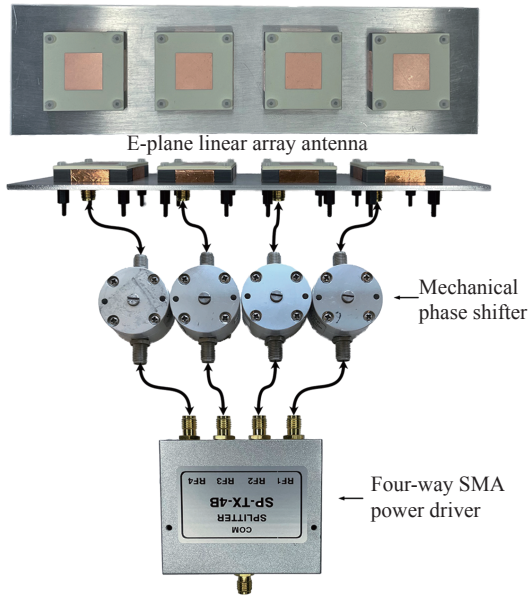

Figure 22 Prototype of the E-plane linear filtering array and measurement.

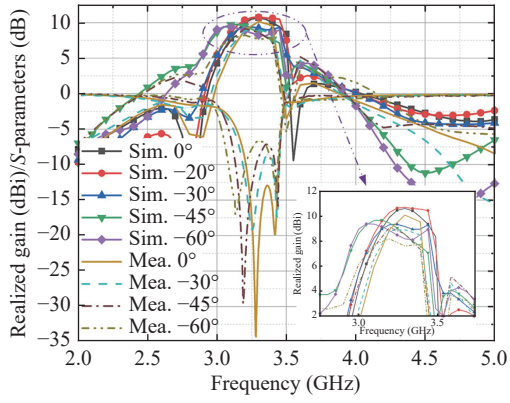

Figure 23 Simulated and measured scanning realized gain and measured scanning reflection coefficients of the E-plane linear filtering array.

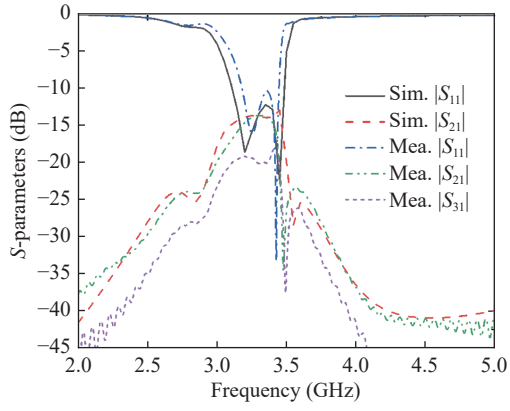

Figure 24 Simulated and measured *S*-parameters of this E-plane linear array.

GHz, which indicate that this array can achieve a beam pattern ranging from −60° to 60° with a low sidelobe and minimal gain reduction, with the worst sidelobe being

−5.5 dB at ±60° beam direction. The cross polarization is lower than −25 dB at any scanning angle, which has a good cross-polarization performance in the E-plane array. The simulation results are verified by the measured results, as depicted in the figure, and display a high degree of consistency. The total efficiency of the E-plane filtering array at different beam directions is presented in Figure 26, which shows that the measured efficiency lies in the range of −0.6 dB to −1.6 dB in the passband and falls below −6 dB in the stopband, indicative of its remarkable filtering characteristics.

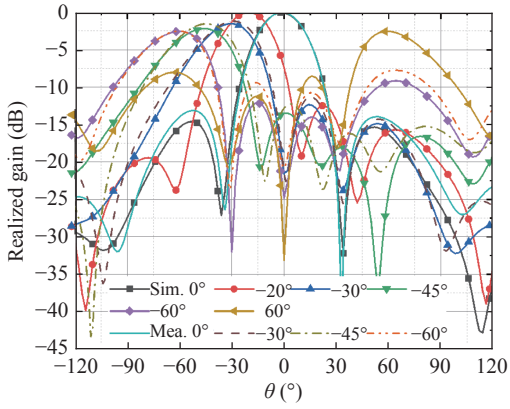

Figure 25 Simulated and measured scanning realized gain and measured scanning reflection coefficients of the E-plane linear filtering array.

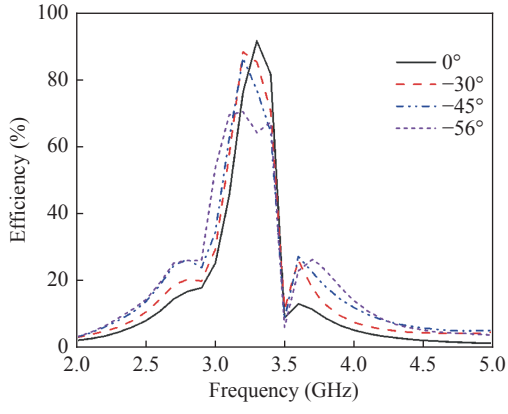

Figure 26 Measured scanning total efficiency of the E-plane linear filtering array.

3. Discussion

The E-plane filtering array boasts a more extensive scanning range in comparison to its H-plane counterpart, as evidenced by its wider E-plane beam-width (as depicted in Figure 13). This observation is substantiated by the analysis presented in (2) and (4). While the H-plane filtering array may offer superior filtering characteristics, the E-plane array experiences a slight degradation in its active impedance matching as a result of coupling, particularly at the edge element. Nevertheless, the proposed method presents a simple and efficient solution for achieving wide-angle beam-scanning with reasonable filtering characteristics in phased arrays. In the case of large-scale arrays, incorporating edge blind elements can mitigate the negative impact of edge elements on the system's performance, leading to improved wide-angle beam-scanning and filtering capabilities.

IV. Conclusion

In summary, to meet the operating scenarios of vehicle communication systems, a new dual-functional FR front-end system is used. The proposed design would be able to achieve the wide beam capability and filtering characteristic through a simple and compact design configuration, which could remarkably reduce the volume and cost of the RF front-end system. Two filtering array systems have been applied to verify the proposed technical contributions, which include the beam scanning capability for coverage of 112° and 120° with a lower gain reduction and the filtering characteristic to improve signal interference. The antenna system is fabricated and measured in the frequency band from 3.18 to 3.45 GHz (about 8.1%), with excellent agreement between simulations and experiments. In light of these promising results, the proposed design is an excellent multifunctional RF front-end system for vehicle communication systems.

Acknowledgement

This work is supported by the National Natural Science Foundation of China (Grant No. 62271412) and the Natural Science Basic Research Plan in Shaanxi Province of China (Grant No. 2022KJXX-65).

References

[1] A. Osseiran, F. Boccardi, V. Braun, *et al.*, "Scenarios for 5G mobile and wireless communications: The vision of the METIS project," *IEEE Communications Magazine*, vol. 52, no. 5, pp. 26–35, 2014.

[2] H. H. Yang, J. C. Shang, J. J. Li, *et al.*, "Multi-Traffic Targets Tracking Based on anImproved Structural Sparse Representation with Spatial-Temporal Constraint," *Chinese Journal of Electronics*, vol. 31, no. 2, pp. 266–276, 2022.

[3] K. Mahler, W. Keusgen, F. Tufvesson, *et al.*, "Tracking of wideband multipath components in a vehicular communication scenario," *IEEE Transactions on Vehicular Technology*, vol. 66, no. 1, pp. 15–25, 2017.

[4] J. D. Gibson, *Mobile Communications Handbook*. CRC Press, Boca Raton, 2012.

[5] K. L. Chung, L. Q. Chen, G. M. Lai, *et al.*, "Three-element circularly polarized MIMO antenna with self-decoupled probing method for B5G-V2X communications," *Alexandria Engineering Journal*, vol. 70, pp. 553–567, 2023.

[6] M. Noor-A-Rahim, Z. L. Liu, H. Lee, *et al.*, "6G for vehicle-to-everything (V2X) communications: Enabling technologies, challenges, and opportunities," *Proceedings of the IEEE*, vol. 110, no. 6, pp. 712–734, 2022.

[7] B. T. Feng, J. Y. Chen, S. X. Yin, *et al.*, "A tri-polarized antenna with diverse radiation characteristics for 5G and V2X communications," *IEEE Transactions on Vehicular Technology*, vol. 69, no. 9, pp. 10115–10126, 2020.

[8] J. F. Zhu, Y. Yang, S. F. Li, *et al.*, "Dual-band dual circularly polarized antenna array using FSS-integrated polarization rotation AMC ground for vehicle satellite communications," *IEEE Transactions on Vehicular Technology*, vol. 68, no. 11, pp. 10742–10751, 2019.

[9] C. X. Mao, S. Gao, and Y. Wang, "Dual-band full-duplex Tx/Rx antennas for vehicular communications," *IEEE Transactions on Vehicular Technology*, vol. 67, no. 5, pp. 4059–4070, 2018.

[10] L. Ge, S. Gao, Y. J. Li, *et al.*, "A low-profile dual-band an-

tenna with different polarization and radiation properties over two bands for vehicular communications," *IEEE Transactions on Vehicular Technology*, vol. 68, no. 1, pp. 1004–1008, 2019.
[11] K. Min, S. Park, Y. Jang, *et al.*, "Antenna ratio for sum-rate maximization in full-duplex large-array base station with half-duplex multiantenna users," *IEEE Transactions on Vehicular Technology*, vol. 65, no. 12, pp. 10168–10173, 2016.
[12] Y. Han, W. K. Tang, S. Jin, *et al.*, "Large intelligent surface-assisted wireless communication exploiting statistical CSI," *IEEE Transactions on Vehicular Technology*, vol. 68, no. 8, pp. 8238–8242, 2019.
[13] G. W. Yang and S. Zhang, "A dual-band shared-aperture antenna with wide-angle scanning capability for mobile system applications," *IEEE Transactions on Vehicular Technology*, vol. 70, no. 5, pp. 4088–4097, 2021.
[14] Y. H. Xu, K. M. Luk, A. Li, *et al.*, "A novel compact magneto-electric dipole antenna for millimeter-wave beam steering applications," *IEEE Transactions on Vehicular Technology*, vol. 70, no. 11, pp. 11772–11783, 2021.
[15] R. Wang, B. Z. Wang, X. Ding, *et al.*, "Planar phased array with wide-angle scanning performance based on image theory," *IEEE Transactions on Antennas and Propagation*, vol. 63, no. 9, pp. 3908–3917, 2015.
[16] Y. Q. Wen, B. Z. Wang, and X. Ding, "Wide-beam SIW-slot antenna for wide-angle scanning phased array," *IEEE Antennas and Wireless Propagation Letters*, vol. 15, pp. 1638–1641, 2016.
[17] G. W. Yang, J. Y. Li, S. G. Zhou, *et al.*, "A wide-angle E-plane scanning linear array antenna with wide beam elements," *IEEE Antennas and Wireless Propagation Letters*, vol. 16, pp. 2923–2926, 2017.
[18] S. Q. Xiao, C. R. Zheng, M. Li, *et al.*, "Varactor-loaded pattern reconfigurable array for wide-angle scanning with low gain fluctuation," *IEEE Transactions on Antennas and Propagation*, vol. 63, no. 5, pp. 2364–2369, 2015.
[19] M. Wang, S. H. Xu, N. Hu, *et al.*, "Design and measurement of a *Ku*-band pattern-reconfigurable array antenna using 16 O-slot patch elements with p-i-n diodes," *IEEE Antennas and Wireless Propagation Letters*, vol. 19, no. 12, pp. 2373–2377, 2020.
[20] Z. J. Chen, Z. Y. Song, H. W. Liu, *et al.*, "A compact phase-controlled pattern-reconfigurable dielectric resonator antenna for passive wide-angle beam scanning," *IEEE Transactions on Antennas and Propagation*, vol. 69, no. 5, pp. 2981–2986, 2021.
[21] L. Gu, Y. W. Zhao, Q. M. Cai, *et al.*, "Scanning enhanced low-profile broadband phased array with radiator-sharing approach and defected ground structures," *IEEE Transactions on Antennas and Propagation*, vol. 65, no. 11, pp. 5846–5854, 2017.
[22] G. W. Yang, J. Y. Li, R. Xu, *et al.*, "Improving the performance of wide-angle scanning array antenna with a high-impedance periodic structure," *IEEE Antennas and Wireless Propagation Letters*, vol. 15, pp. 1819–1822, 2016.
[23] R. L. Xia, S. W. Qu, P. F. Li, *et al.*, "Wide-angle scanning phased array using an efficient decoupling network," *IEEE Transactions on Antennas and Propagation*, vol. 63, no. 11, pp. 5161–5165, 2015.
[24] P. Cheong, K. F. Chang, W. W. Choi, *et al.*, "A highly integrated antenna-triplexer with simultaneous three-port isolations based on multi-mode excitation," *IEEE Transactions on Antennas and Propagation*, vol. 63, no. 1, pp. 363–386, 2015.
[25] C. X. Mao, S. Gao, Y. Wang, *et al.*, "Compact highly integrated planar duplex antenna for wireless communications," *IEEE Transactions on Microwave Theory and Techniques*, vol. 64, no. 7, pp. 2006–2013, 2016.
[26] Y. Zhang, X. Y. Zhang, and Q. H. Liu, "A six-port dual-function RF device with four-element MIMO antenna array and bandpass filter operations," *IEEE Transactions on Antennas and Propagation*, vol. 68, no. 6, pp. 4549–4559, 2020.
[27] W. C. Yang, M. Z. Xun, W. Q. Che, *et al.*, "Novel compact high-gain differential-fed dual-polarized filtering patch antenna," *IEEE Transactions on Antennas and Propagation*, vol. 67, no. 12, pp. 7261–7271, 2019.
[28] S. J. Yang, Y. M. Pan, L. Y. Shi, *et al.*, "Millimeter-wave dual-polarized filtering antenna for 5G application," *IEEE Transactions on Antennas and Propagation*, vol. 68, no. 7, pp. 5114–5121, 2020.
[29] G. Liu, Y. M. Pan, and X. Y. Zhang, "Compact filtering patch antenna arrays for marine communications," *IEEE Transactions on Vehicular Technology*, vol. 69, no. 10, pp. 11408–11418, 2020.
[30] W. B. Pan, C. Huang, P. Chen, *et al.*, "A beam steering horn antenna using active frequency selective surface," *IEEE Transactions on Antennas and Propagation*, vol. 61, no. 12, pp. 6218–6223, 2013.
[31] G. W. Yang, J. Y. Li, J. J. Yang, *et al.*, "A wide beamwidth and wideband magnetoelectric dipole antenna," *IEEE Transactions on Antennas and Propagation*, vol. 66, no. 12, pp. 6724–6733, 2018.
[32] D. M. Pozar, "The active element pattern," *IEEE Transactions on Antennas and Propagation*, vol. 42, no. 8, pp. 1176–1178, 1994.
[33] Spectrum Control, "980 coaxial phase shifter," Available at: https://www.apitech.com/products//rf-solutions/phase-shifters/980-coaxial-phase-shifters/.

Chuang HAN received the B.S., M.S. and Ph.D. degrees in electronic engineering from Northwestern Polytechnial University (NPU), Xi'an, China, in 2012, 2015 and 2019, respectively. Currently, he works as an Associate Researcher at NPU. His recent research interests include array signal process, antenna analysis and synthesis, satellite communication systems, and satellite navigation systems.

Tong LI received the B.S. and M.S. degrees from NPU in 2016 and 2019, respectively. She is currently pursuing the Ph.D. degree at NPU. Her current research interests include wireless communications and satellite communications.

Zhaolin ZHANG received the B.S., M.S., and Ph.D. degrees from NPU in 2000, 2005, and 2012, respectively. He is an Associate Professor with NPU. His research interests include antenna array processing, adaptive antijamming, and multimedia communication.

Ling WANG received the B.S., M.S., and Ph.D. degrees in electronic engineering from Xidian University, Xi'an, China, in 1999, 2002, and 2004, respectively. From 2004 to 2007, he was with Siemens and Nokia Siemens Networks, Espoo, Finland. Since 2007, he has been with NPU as a Professor. Currently, he serves as the Dean of School of Electronics and Information. His current research interests include array processing and smart antennas, wideband communications, cognitive radio, adaptive anti-jamming for satellite communications, satellite navigation, and date link systems.

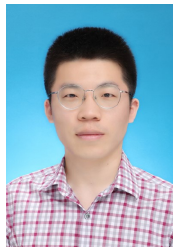

Guangwei YANG received the B.E., M.S., and Ph.D. degrees all in electronic engineering in NPU in 2012, 2015, 2019, respectively. He is currently working at Queen Mary University of London as a Royal Society-Newton International Fellow. He was a Postdocal Researcher in the Antenna, Propagation and Millimeter-wave Systems (APMS) Section, Aalborg University, Denmark from 2019 to 2020. He also serves as a Reviewer for all the IEEE and IET journals related to antennas. His recent research interests include advanced antenna systems, multi-beam antennas, phased array, lens antennas, mm-wave array antennas for wireless communication, wireless communication, microwave and optical metamaterials, and spatial modulation. (Email: gwyang086@gmail.com)